SUPPLEMENTARY INFORMATION

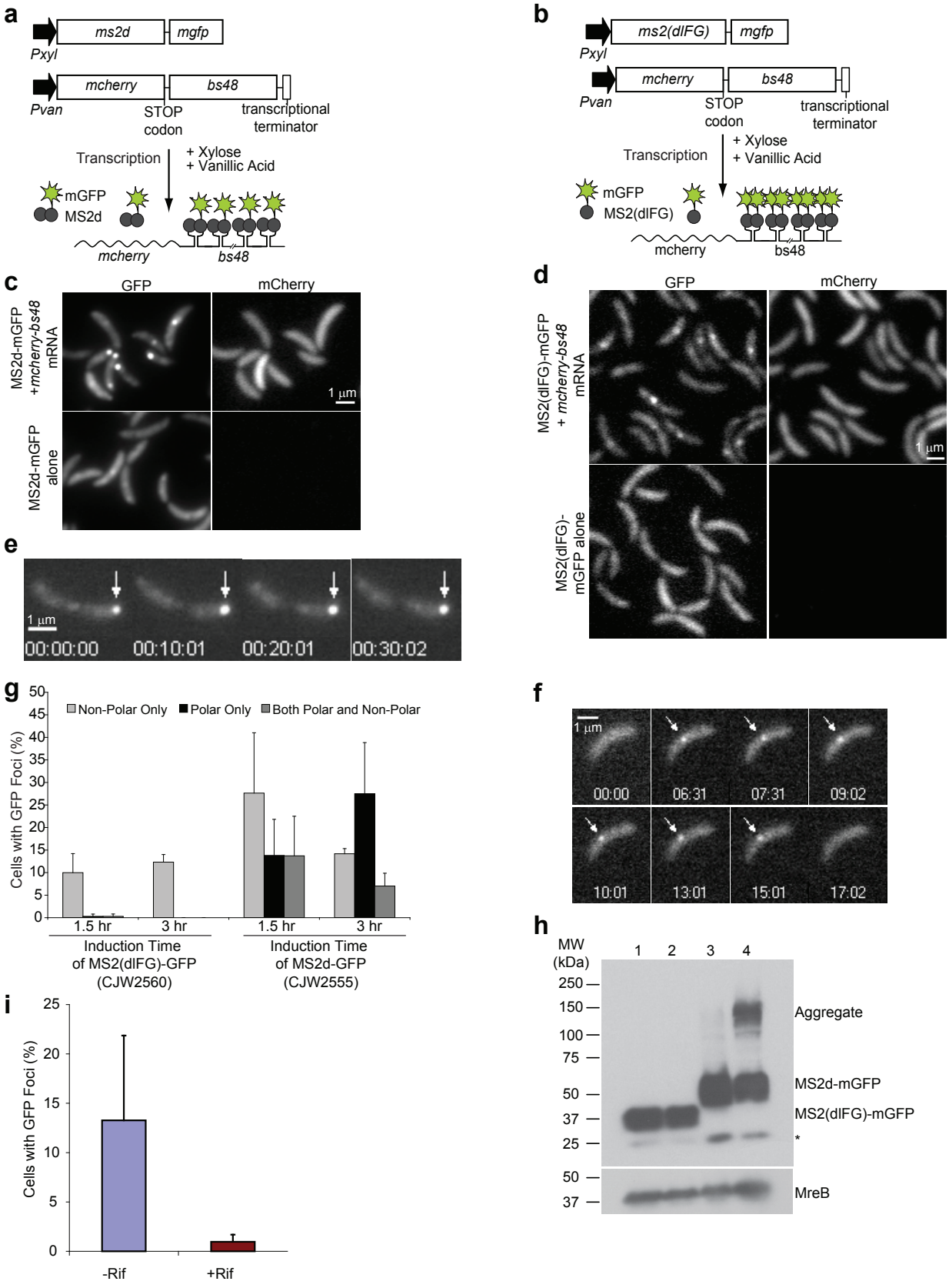

Supplementary Fig. 1. The assembly-defective RNA-binding protein MS2(dlFG) is better suited than MS2d to visualize transcripts in *C. crescentus*. **a,** Schematic representation of the methodology and genetic background of strain CJW2555. In this strain, a gene encoding an MS2d-mGFP fusion was placed on the chromosome under the control of the xylose-inducible

promoter *Pxyl* while *mcherry* transcriptionally fused to 48 MS2 binding sites (*bs48*) at the 3' end was encoded from the vanillic acid-responsive promoter *Pvan* at the chromosomal *vanA* locus. **b,** Schematic representation of the methodology and genetic background of strain CJW2560. As in (*a*) except that *Pxyl* expresses MS2(dlFG)-mGFP, instead of MS2d-mGFP. **c,** *Top panels*, fluorescent images of CJW2555 cells producing MS2d-mGFP and *mcherry-bs48* mRNA by growing in the presence of xylose and vanillic acid for 1.5 h. *Bottom panels*, fluorescent images of control CJW2780 cells producing MS2d-mGFP only (i.e., there is no inserted *mcherry-bs48* construct in this strain). Images were acquired using the GFP (*left*) and mCherry (*right*) filter sets. MS2d-mGFP displayed a largely diffuse signal in the cytoplasm in control CJW2780 cells. However, fluorescent foci appeared in some CJW2555 cells when MS2d was co-produced with *mcherry-bs48* mRNA. These foci were found internally or at cell poles. Fluorescent mCherry signal was detected in the cytoplasm in CJW2555 cells, consistent with production of mCherry protein. **d,** As in (*c*), except that the top panels shows CJW2560 cells producing MS2(dlFG)-mGFP and *mcherry-bs48* mRNA, and the bottom panels show control CJW2556 cells producing MS2(dlFG)-mGFP alone (i.e., there is no inserted *mcherry-bs48* construct). MS2(dlFG)-mGFP displayed a largely diffuse signal in the cytoplasm in control CJW2556 cells. However, fluorescent foci appeared in some CJW2560 cells when MS2(dlFG)-mGFP was co-produced with *mcherry-bs48* mRNA. These foci were found internally and not at the cell poles. Fluorescent mCherry signal was detected in the cytoplasm in CJW2560 cells, indicating mCherry production. **e,** Time-lapse microscopy of CJW2555 cells producing MS2d-mGFP and *mcherry-bs8* mRNA after 1.5 h growth in liquid culture at 30˚C in the presence of xylose and vanillic acid. The agarose pad also contained vanillic acid (and no xylose). Images were taken at 30-sec intervals for 30 min at room temperature; only selected images from this time-lapse sequence are shown (h:min:sec). These experiments showed that polar MS2d-mGFP foci (arrow) are long lived. **f,** Time-lapse microscopy of CJW2560 cells growing on an agarose padded-slide containing vanillic acid to maintain expression of *mcherry-bs48* mRNA. Prior to microscopy, the cells were grown in a liquid culture in the presence of xylose and vanillic acid for 1.5h to produce MS2(dlFG)-mGFP and *mcherry-bs48* mRNA, respectively. Shown are selected images of a representative cell in which a GFP focus appeared and disappeared within 17 min of the time-lapse sequence. **g,** Quantification of CJW2555 and CJW2560 cells with internal (non-polar) and polar GFP foci after 1.5 and 3 h of induction with 0.03% xylose and 0.5 mM vanillic acid. CJW2555 cells producing MS2d-mGFP and *mcherry-bs48* form both polar and non-polar GFP foci, and the proportion of polar foci increased with induction time of MS2d-mGFP synthesis. By contrast, CJW2560 cells producing MS2(dlFG)-mGFP and *mcherry-bs48* only formed non-polar foci, irrespective of the induction time of MS2(dlFG)-mGFP. Quantification was performed using spotFinder. N = 3 experiments; ≥101 cells for each time-point. Error bars represent the standard deviation. **h,** Western blot of protein extracts from cells producing either MS2d-mGFP (CJW2555) or assembly-defective MS2(dlFG)-mGFP (CJW2560), in the presence or absence of *mcherry-bs48* mRNA. CJW2560 cells were grown in the presence of 0.3% xylose for 5 h to produce high levels of MS2(dlFG)-mGFP, and without (lane 1) or with (lane 2) 0.5 mM vanillic acid for 5 h to express *mcherry-bs48* mRNA. CJW2555 cells were grown under identical conditions to produce MS2d-mGFP in the absence (lane 3) or presence (lane 4) of *mcherry-bs48* mRNA. SDS-PAGE followed by Western blot analysis using anti-GFP antibodies revealed that MS2d-mGFP, unlike MS2(dlFG)-mGFP, tends to make stable aggregates when co-produced with *mcherry-bs48* mRNA. Asterisk shows a minor degradation product. Probing the same membrane with anti-MreB antibodies provided a loading control. **i,** Quantification of GFP foci in CJW2560 cells producing MS2(dlFG)-mGFP and *mcherry-bs48* mRNA after 1.5h of xylose and vanillic acid induction before (blue) and after (crimson) treatment with rifampicin (25 μg/ml) for 20 min. Foci were detected using spotFinder. N = 3 experiments; ≥364 cells for each experiment without rifampicin and ≥179 cells for each experiment with rifampicin.

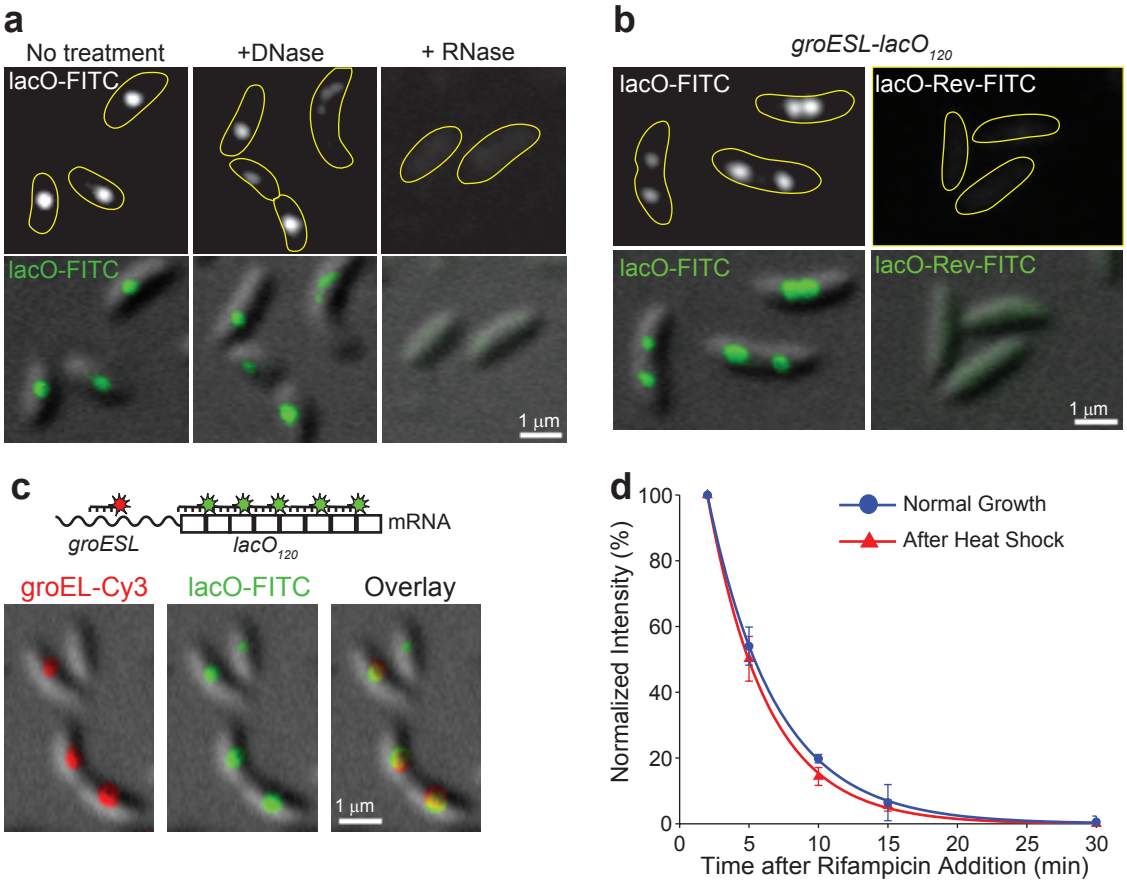

Supplementary Fig. 2. Validation of the lacO method. **a**, Visualization of *groESL-lacO*$_{120}$ mRNA-expressing CJW2966 cells using lacO-FITC LNA probe before (left) or after treatment with DNase I (middle) or RNase A (right). **b**,RNA FISH microscopy of *groESL-lacO*$_{120}$ mRNA-expressing CJW2966 cells using lacO-FITC or the complementary probe, lacO-Rev-FITC. **c**, Visualization of *groESL-lacO*$_{120}$ mRNAs in CJW2966 cells using groEL-Cy3 and lacO-FITC probes. **d**, Decay fit of the *groESL-lacO*$_{120}$ mRNA signal (detected with the lacO-Cy3 probe) in CJW2966 cells after rifampicin addition. Cells were grown at 30°C (blue) or 42°C (red) for 15 min before rifampicin addition. Error bars indicate standard deviation from 2 independent experiments (>245 cells for each time point).

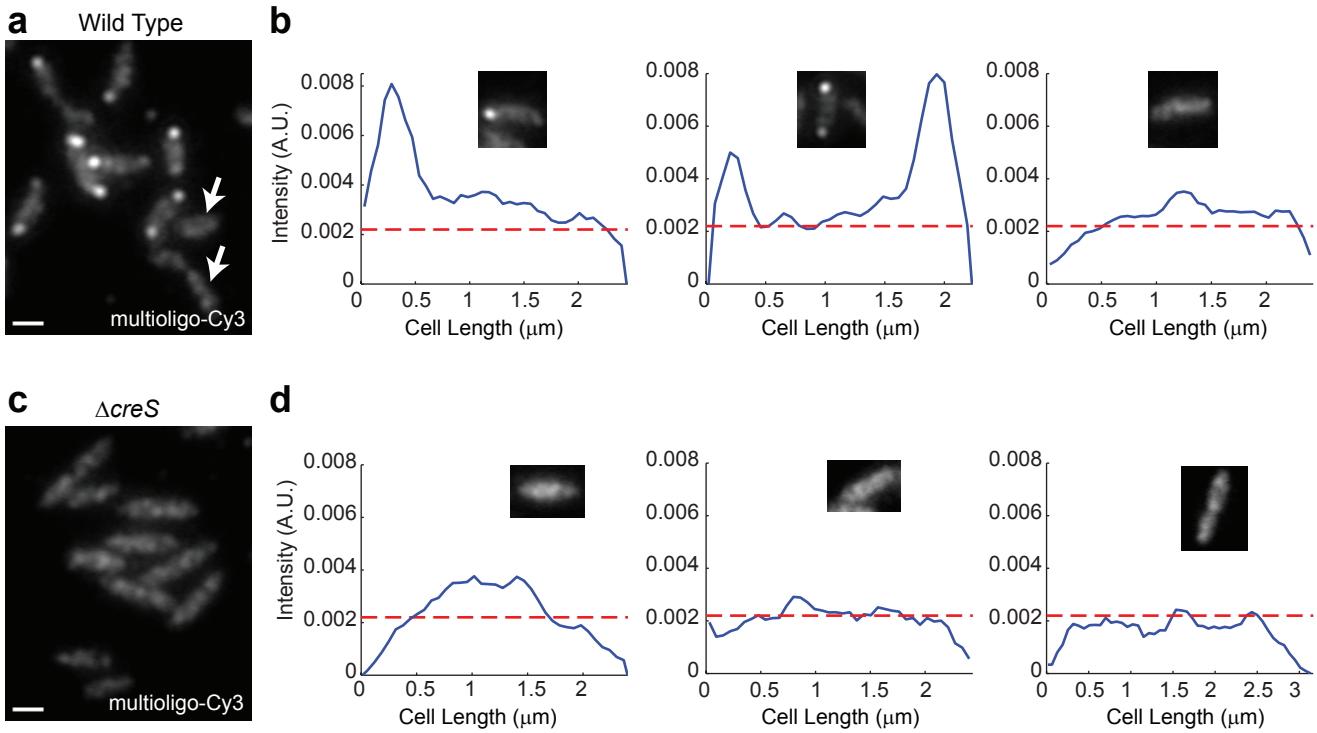

Supplementary Fig. 3. Visualization of endogenous *creS* mRNA by FISH. **a**, Visualization of native *creS* mRNA in wild-type CB15N cells by RNA-FISH using 38 Cy3-labeled DNA probes that hybridize in tandem to the *creS* mRNA sequence. Arrows show wild-type cells with a pattern of fluorescent signal similar to that of ΔcreS cells (see panel c). **b**, Representative fluorescent intensity profiles of individual wild-type cells exhibiting either one (left), two (center), or zero (right) polar accumulation(s). The red dashed line represents the average background fluorescence determined from the signal intensity obtained from Δ*creS* cells treated under identical conditions (see panel c). **c**, Visualization of background fluorescence in Δ*creS* cells (negative control) due to unspecific probe binding and cellular autofluorescence using conditions as in (a). **d**, Representative fluorescent intensity profiles of individual Δ*creS* cells. The red dashed line represents the average background fluorescence in Δ*creS* cells.

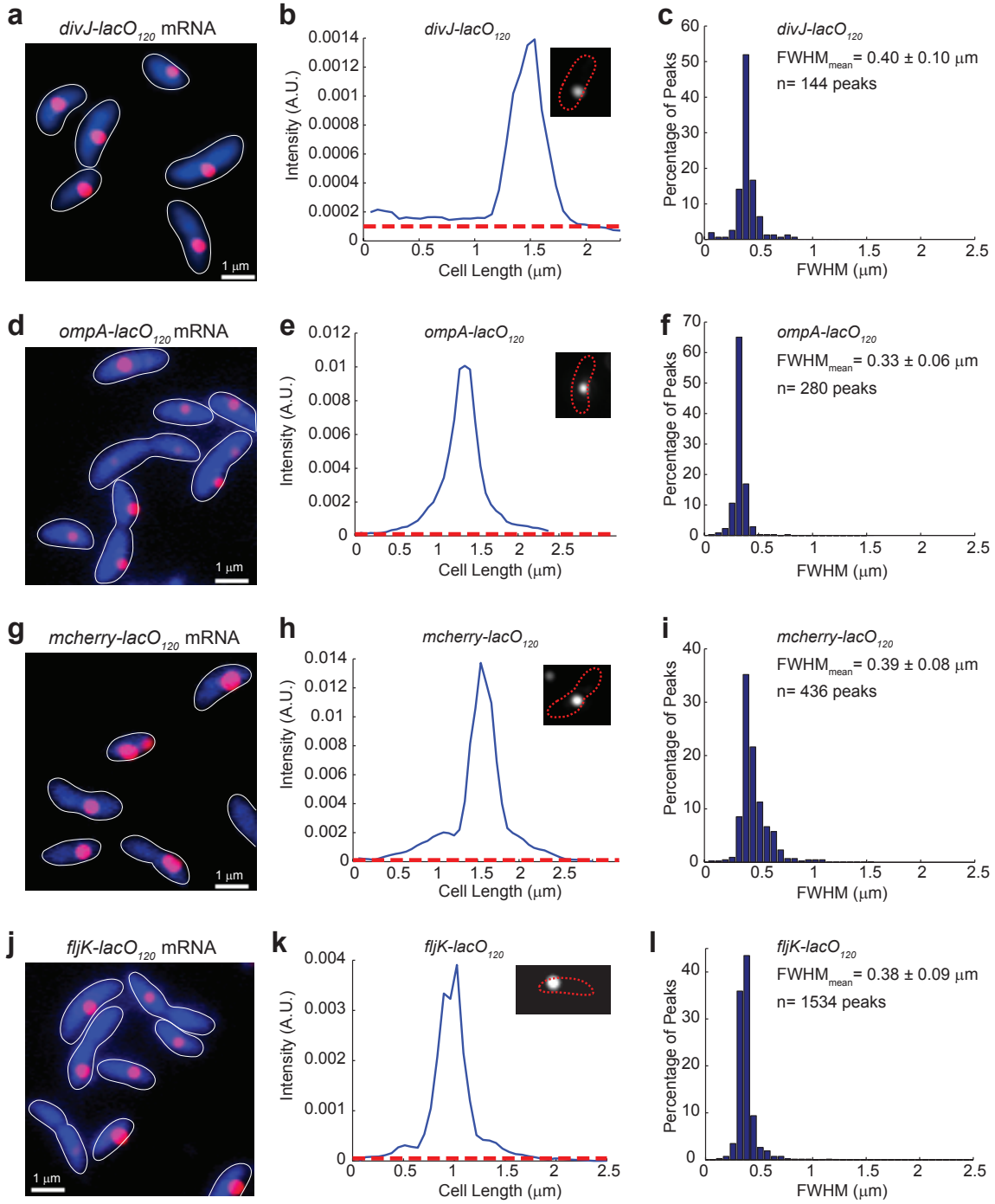

Supplementary Fig. 4. Limited dispersion of mRNA is common. **a**, Visualization of *divJ-lacO*$_{120}$ mRNA in CJW2968 cells by RNA FISH using the lacO-Cy3 probe. **b**, Representative intensity profiles of *divJ-lacO*$_{120}$ mRNA (hybridized with the lacO-Cy3 probe) along the cell length in individual CJW2968 cells. The red dashed line corresponds to the measured background fluorescence. **c**, *divJ-lacO*$_{120}$ mRNA dispersion inside cells was determined by plotting the distribution of FWHM values for each peak obtained from intensity profiles of CJW2968 cells. **d-f**, Same as (**a-c**) for *ompA-lacO*$_{120}$ mRNA in CJW3093 cells. **g-i**, Same as (**a-c**) for *mcherry-lacO*$_{120}$ mRNA in CJW3097 cells after 10 min of induction with 0.5 mM vanillic acid. **j-l**, Same as (**a-c)** for flagellin *fljK- lacO*$_{120}$ mRNA in CJW3364cells.

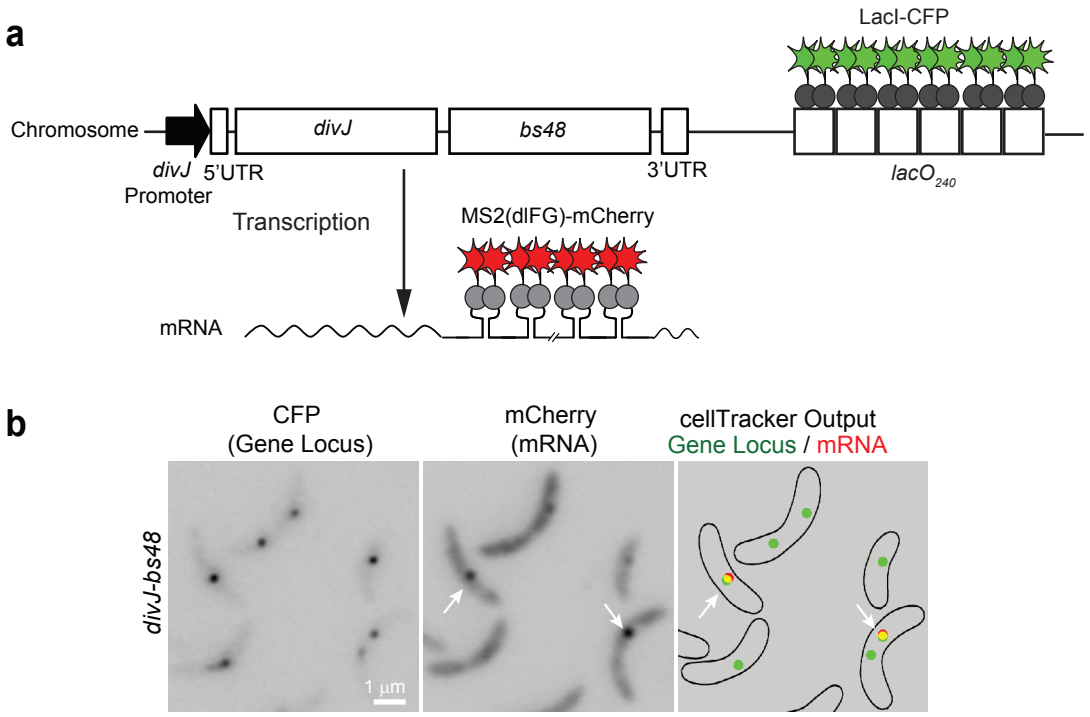

Supplementary Fig. 5. *divJ-bs48* mRNA foci colocalize with *divJ* gene loci. **a**, Schematic representation of the methodology and genetic background used to simultaneously visualize *divJ* mRNA and gene locus. In strain CJW2783, *divJ* is transcriptionally tagged with bs48, allowing visualization of the resulting mRNA using MS2(dlFG)-mCherry produced from P*xyl* at the chromosomal *xylX* locus. This strain also contains a $lacO_{240}$ array inserted nearby the *divJ-bs48* gene, which can be used to visualize this gene locus by DNA binding of LacI-CFP also produced from P*xyl*. **b**, Inverted fluorescence images of CJW2783 cells grown in the presence of xylose for 1h to induce the synthesis of both MS2(dlFG)-mCherry and LacI-CFP. The foci corresponding to MS2(dlFG)-mCherry-labeled *divJ-bs48* mRNA (middle) colocalize with LacI-CFP foci representing chromosomal loci (left). The right panel displays processed images from cellTracker and spotFinder analysis, showing cell outlines and identified mRNA foci (red), gene loci (green), and overlap (yellow). Arrows indicate mRNA foci appearing at or near corresponding gene loci.

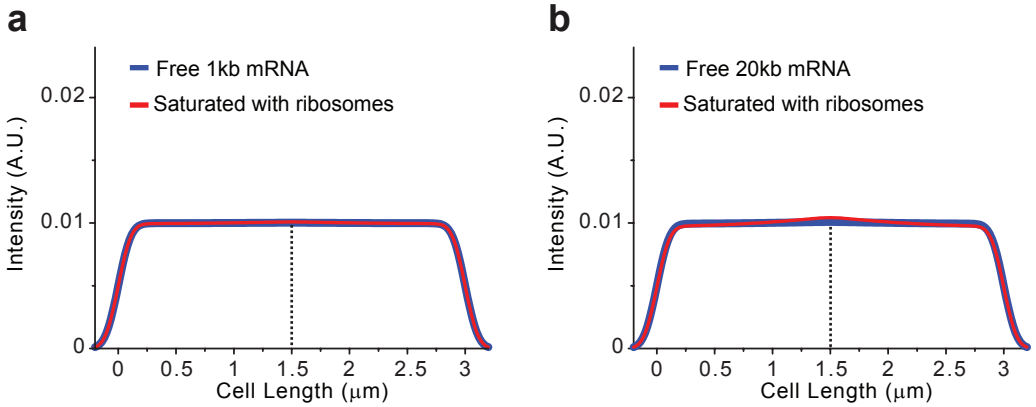

Supplementary Fig. 6. Calculated mRNA distribution profiles show a largely uniform spatial distribution inside cells, regardless of mRNA size or ribosome occupancy. Calculated mRNA distribution profiles in a 3-μm virtual cell. Profiles were calculated with Eq.[6] (see Supporting Information) for (**a**) 1-kb mRNA (commonsize) and (**b**) 20-kb mRNA (illustrating long polycistronic transcripts), either free of ribosome (blue) or saturated with ribosomes (red). The dotted line delineates the source of mRNA (site of transcription) located at the 1.5-μm position. The model assumes a rate of transcription of 0.06 s^{-1} and a rate of mRNA degradation of 0.004 s^{-1} (which corresponds to a half-time of 3.5 min). These values resulted in a total of 15 mRNAs of interest per cell.

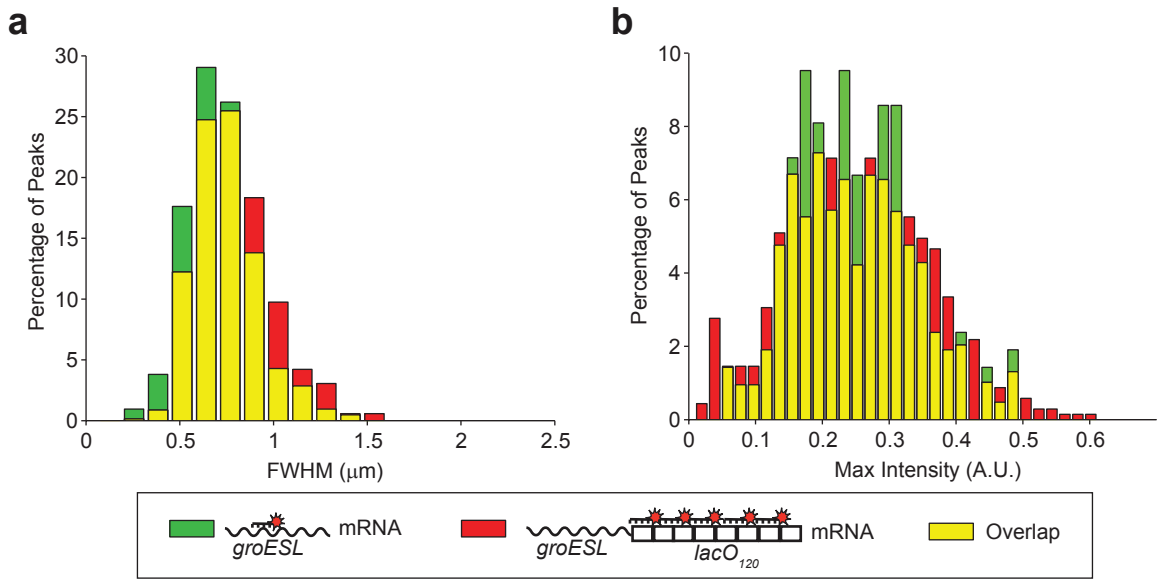

Supplementary Fig. 7. Comparison of dispersion and intensity distributions for *groESL* and *groESL-lacO*$_{120}$ after heat shock. **a**, The distribution of *groESL-lacO*$_{120}$ mRNA dispersion (based on FWHM values) in heat shock-treated CJW2966 cells using the lacO-Cy3 probe (red) is similar to that of natural *groESL* mRNA dispersion in wild-type, heat shock-treated cells using a groEL-Cy3 probe (green). Overlapping distribution is in yellow. **b**, Similarly, the distribution of *groES-lacO*$_{120}$ mRNA levels (maximal fluorescence intensities) in heat shock-treated CJW2966 cells using the lacO-Cy3 probe (red) is, after normalization by the mean fluorescence intensity, similar to that of natural *groESL* mRNA levels in wild-type, heat shock-treated cells using the groEL-Cy3 probe (green).

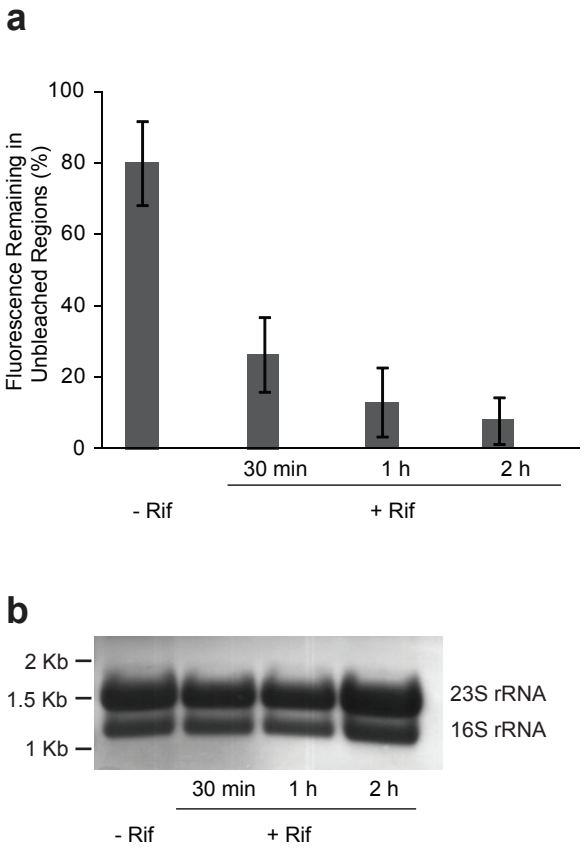

Supplementary Fig. 8. Mobility of L1-GFP is affected by rifampicin treatment. **a**, Quantification of fluorescence remaining in unbleached cellular regions after 10-s photobleaching of cell poles in the absence of rifampicin (n = 14 cells) or after 30 min (n = 22 cells), 1 h (n = 34 cells), and 2 h (n = 18 cells) of rifampicin treatment. Error bars represent the standard deviation. **b**, Methylene blue staining of total RNA extracted from untreated cells, and after rifampicin treatment for 30 min, 1 h or 2 h.

SUPPLEMENTAL TEXT

Visualization of mRNA in live *C. crescentus* cells. A method to visualize mRNA in living eukaryotic cells was first developed in yeast, using a GFP-tagged RNA-binding protein, MS2, to label an array of MS2 binding sites transcriptionally fused to the mRNA of interest[1]. This approach was adapted for *E. coli,* notably by increasing the number of MS2 binding sites to amplify the bound fluorescent signal and by using a dimeric variant of MS2 (MS2d)[2]. While this method has shown great value in quantifying transcriptional bursting[3], it resulted in persistence of the MS2d-GFP signal throughout the cell's lifetime[2,3], inconsistent with the typically short halftime of bacterial mRNAs[4]. Since MS2 is a bacteriophage coat protein that is capable of self-assembly into a phage capsid, we suspected that immortalization of the fluorescent signal may be caused by self-aggregation of MS2d-GFP when mRNA binding brings subunits in close proximity. To test this idea, we attempted to visualize chromosomally expressed *mcherry* mRNAs tagged with 48 MS2 binding sites (*bs48*) in *C. crescentus* using either MS2d (Supplementary Fig. 1a) or an assembly-defective MS2 [MS2(dlFG)] mutant[5] (Supplementary Fig.1b), which is commonly used in eukaryotic mRNA studies. Each MS2 variant was fused to a monomeric version of GFP (mGFP). *mcherry-bs48* and the mGFP-tagged MS2 variant were each produced from the chromosome under inducible promoters *Pvan* and *Pxyl*, respectively (Supplementary Fig. 1a-b).

Synthesis of MS2d-mGFP in *mcherry-bs48* mRNA-expressing cells generated bright fluorescent foci with long lifespans (Supplementary Fig. 1c, e) in 60% of cells (n=1527). Conversely, MS2(dlFG)-mGFP gave weak, short-lived fluorescent foci in 16% of cells (n=559; Supplementary Fig.1d) that appeared and disappeared over time (Supplementary Fig. 1f). Using the assembly-capable MS2d-mGFP also caused inconsistent results with respect to the localization of fluorescent foci. When *mcherry*-bs48 mRNA and MS2-mGFP were produced, the cells displayed non-polar and/or polar fluorescent foci (Supplementary Fig. 1c). Polar localization became predominant with increased MS2d-mGFP levels (Supplementary Fig. 1g; n = 3 experiments, ≥101 cells for each time-point). On the other hand, GFP foci formed from assembly-defective MS2(dlFG)-mGFP almost exclusively exhibited non-polar localization (Supplementary Fig. 1d), and the localization pattern did not change significantly between 1.5 h and 3 h

induction of MS2(dlFG)-mGFP synthesis (Supplementary Fig. 1g; n = 3 experiments, ≥106 cells for each time point). FISH experiments described in the main text (Supplementary Fig. 3g) confirmed that the polar localization of MS2d-mGFP foci was artefactual, possibly because aggregates tend to accumulate at the cell poles[6,7]. Western blot analysis confirmed that MS2d-mGFP, unlike MS2(dlFG)-mGFP, had the capability of forming in vivo aggregates when *mcherry-bs48* mRNAs were expressed (Supplementary Fig. 1h). The fluorescent foci generated in some cells when both MS2(dlFG)-mGFP and *mcherry-bs48* mRNA were produced corresponded to MS2(dlFG)-mGFP-bound mRNA signal as they were virtually absent in mRNA-depleted cells after treatment with the transcriptional initiation inhibitor rifampicin (Supplementary Fig. 1i). While using MS2(dlFG)-mGFP to label mRNAs was clearly the better choice for qualitative visualization of mRNA in *C. crescentus*, the significant background fluorescence caused by unbound MS2(dlFG)-mGFP masked some bs48-tagged mRNAs, preventing us from quantifying the spatial distribution of mRNA. The signal-to-noise ratio could not be sufficiently improved by varying the expression level of MS2(dlFG)-mGFP. This is likely due to the poor binding capability of MS2(dlFG) to its target RNA sequences when fused to a fluorescent protein. Consistent with this interpretation, it has been shown in vivo using a blue-white colony assay[8] that unlike MS2d-GFP, a GFP fusion to MS2(dlFG) is unable to repress the translation of the MS2 replicase fused to β-galactosidase fusion[2]. Because of these caveats, we turned to RNA FISH for our analysis.

Visualization of endogenous mRNAs in wild-type cells using RNA FISH and multiple DNA probes

A single LNA probe of 17 nt complementary to native mRNA in wild-type CB15N cells typically did not provide enough sensitivity for visualization (except for the naturally abundant *groESL* mRNA; Fig. 1a). Therefore, to enhance detection of native mRNA, we used multiple Cy3-labeled DNA probes that bind in tandem to the target mRNA, as previously described[9-11]. We visualized *creS* mRNA because its gene locus is in close proximity to the origin and thus expected to be polarly localized. A *creS* deletion strain was used to assess nonspecific probe binding. Hybridization of 38 Cy3-labeled DNA

probes of 25 to 30 nt of length (see list below) to the *creS* mRNA sequence showed accumulation of fluorescent signal to one or both cell poles in many wild-type cells (Supplementary Fig. 3a and b, left and center graphs). A fraction of wild-type cells displayed an uneven but largely dispersed signal (Supplementary Fig. 3a, arrows; and Supplementary Fig. 3b, right graph) that was similar to the unspecific signal observed in all Δ*creS* cells hybridized under identical conditions (Supplementary Fig. 3c and d, all 3 graphs). For quantification and assessment of the signal-to-noise ratio, we determined the average background signal (red dotted line in Supplementary Fig. 3b and d) due to nonspecific probe binding and cell autofluorescence by calculating the mean of the fluorescence intensity in Δ*creS* cells (n=2098 cells) normalized by the cell area. Fluorescence intensity profiles along the cell length clearly showed that the polar signal in wild-type cells was well above background (Supplementary Fig. 3b), in striking contrast to the signal of Δ*creS* cells (Supplementary Fig. 3d). The polar *creS* mRNA peaks in wild-type cells were diffraction-limited (FWHM=0.37±0.14 μm; n=338 peaks), confirming that native *creS* mRNAs display limited dispersion from their site of synthesis, which further validates the lacO tagging method (Fig. 2d). It should be noted that comparatively to the 38-probe approach, the lacO method gives a higher signal-to-noise ratio. In the lacO method, one single LNA probe hybridizes up to 120 equivalent sites whereas in the multiprobe method, 38 distinct probes hybridize to 38 different sites. Thus, there are more binding sites in the lacO method. Additionally, the background fluorescence is about 6 times higher when using 38 DNA probes relative to one single LNA lacO probe because increasing the number of probes to improve the fluorescence signal also has the detrimental effect of increasing unspecific binding.

To expand and generalize our findings, we used the multi-probe approach to examine the localization of LacZ-encoding mRNA in wild-type MG1665 *E. coli* cells during non-induced or induced conditions. We used 48 Cy3-labeled probes complementary to the *lacZ* coding region. We showed that after induction with IPTG, *lacZ* containing mRNA is localized as 1 or 2 spots in wild type cells (Fig.3a), while non-induced cells did not show an accumulation of *lacZ* mRNA signal (Fig.3c). We determined the fluorescence background by calculating the mean of the average fluorescence intensity from non-induced cells (n=1011 cells). Intensity profiles along the

cells length showed an accumulation of fluorescence in one (Fig. 3b *right*) or two (Fig. 3b *left*) peaks that were well above background, as opposed to non-induced cells (Fig. 3d). Measurements of the FWHM of these RNA spots showed that they are diffraction limited (Fig.3 e). Quantification of the percentage of induced cells with RNA spots is shown in Table S2.

Assessment of ribosomal RNA integrity after rifampicin treatment

Total RNA was extracted as previously described[12] from exponentially growing *C. crescentus* cultures immediately after addition of rifampicin, and after treatment for 30 min, 1 h, or 2 h. Five micrograms of total RNA from each sample were loaded into a formaldehyde agarose gel, and the RNA was transferred to a nylon membrane using a downward capillarity transfer system. Ribosomal RNA bands were detected by methylene blue staining (Supplementary Fig. 8b).

IMAGE AND DATA ANALYSIS

Outlining cells and computing fluorescence intensity profiles (MicrobeTracker):

Cells were outlined in phase images using custom-made MATLAB-based program named MicrobeTracker, which will be described in detail in a manuscript in preparation. Briefly, individual cells were identified from phase images by thresholding and using an edge detection routine. The identified cells were then outlined with a continuous contour, which was adjusted using a version of the Point Distribution Model (PDM)[13], using wild-type CB15N cells as a training set. The resulting outline was smoothed using Fourier transform keeping only the first 16 modes. The outline was then used to determine the centerline (skeleton) of the cell. A series of perpendiculars was placed at every pixel along the centerline, thus creating a mesh and splitting the cell into segments along its length.

To obtain fluorescence intensity profiles, the background fluorescence intensity was first computed by averaging fluorescence intensity in cell-free areas of the image and was then subtracted from the image. After applying the cell mesh, the intensity of each segment was integrated and divided by the area of the segment. All operations were

performed in MATLAB using MATLAB standard routines and the Image Processing Toolbox.

Measurements of background cellular fluorescence: A sample of wild-type CB15N cells (which lack the *lacO* array) was included in each RNA FISH experiment that used the lacO probe. This sample, which was treated under the same conditions (including sample preparation and camera settings) as for the strains that contain the $lacO_{120}$ array, served as a negative control to assess unspecific binding of the lacO probe and cellular autofluorescence. This background fluorescence was estimated by determining the mean of the fluorescence intensity normalized by the cell area.

Detecting mRNA/DNA Fluorescence Foci (SpotFinder)

To identify fluorescence foci, we developed another custom-built MATLAB-based program named SpotFinder. This program is based on the idea that foci are equivalent to round, diffraction-limited spots on uneven background. It uses band-pass spatial filtering adjusted to detect only the objects close to diffraction-limited spot sizes. Filtered images were processed using morphological opening in order to eliminate non-spherical features. A histogram of integrated spot intensities was computed and compared to a histogram obtained from control cells. From this comparison, a threshold was calculated such that spots above this threshold include no more than 5% of false positives. Importantly, SpotFinder was only used to find the position of fluorescent spots and construct a mask to be applied to the original image. The integrated fluorescence of each spot was calculated from the original image. SpotFinder was also used to quantify the number of mRNA foci in cells after RNA FISH (see Table S2).

mRNA half-time measurements by FISH

Cell samples at different time points after rifampicin (100 μg/ml) addition were immediately fixed with 4% formaldehyde. RNA FISH was performed as described in the method section. Fluorescence intensity in the cell population was calculated for each time point after rifampicin addition using MicrobeTracker. The background fluorescence obtained from wild-type cells lacking a $lacO_{120}$ array was subtracted from each value.

The corrected values were plotted versus time and fitted using a least squares fit with an exponential function $I = I_0 \exp(-\lambda t) + I_b$ where I_0 is the initial intensity, I_b is the background intensity, and λ is the decay coefficient. Note that the fluorescent intensity values at time 0 and 2 min were similar, which presumably reflects the time for rifampicin to enter the cells and to inhibit transcription. The 0-min values were therefore excluded to allow better curve fitting. The calculated decay coefficients λ for *groESL-lacO*$_{120}$ mRNA under normal growth and after heat shock were 0.21 and 0.23, respectively. The R-square coefficients were 0.9999 and 0.9997, respectively. The calculated half-times using the decay coefficients were 3.48±0.15 min without heat shock and 3.01±0.3 min after heat shock.

mRNA half-time measurements by real-time PCR

The samples of CB15N or CJW2966 exponentially growing cultures at different time points following rifampicin (100 μg/ml) addition were centrifuged for 30 s and the pellets were immediately resuspended in Trizol (Sigma). Total RNA was then extracted as previously described[12] and cDNA was obtained for each sample using High capacity cDNA reverse transcription kit (Applied Biosystems 4368814). The efficiency test for *groESL* and 16s-specific primers and the amplification of the products were performed following the Power SYBR Green PCR protocol (Applied Biosystems) using a 7900HT ABI PRISM Real Time PCR System. The efficiency for *groESL* and 16S-specific primers was determined to be 89.7% and 89.9%, respectively. The relative amount of *groESL* and *groESL-lacO*$_{120}$ mRNAs at each time point was calculated by comparing the threshold cycle (Ct) values obtained using the software analysis tool. The relative decrease in mRNA level between time points after rifampicin addition was calculated using the Pfaffl method[14] using the equation $F = (E_{groESL})^{\Delta Ct} / (E_{16s})^{\Delta Ct}$ where F is the relative difference between time points, E_{groESL} and E_{16s} are the efficiencies for *groESL* and 16S specific primers, respectively. The normalized values were plotted against time and fitted as described above. The calculated decay coefficients λ for *groESL* and *groESL-lacO*$_{120}$ mRNAs under normal growth conditions were 0.15. and 0.17, respectively, and after heat shock were 0.14. and 0.16, respectively. The calculated half-times using the decay coefficients were 4.9 ± 1.6 min and 4.35 ±1.1 min for *groESL* and

groESL-lacO$_{120}$ mRNAs under normal growth, and 5.1 ± 0.6 min and 4.2 ± 0.7 after heat shock, respectively. The differences in half-time values were found to be not statistically different using the one-way ANOVA test from MATLAB Statistics Toolbox (*p*-value 0.703).

Note that the small difference between half-time values obtained by RNA FISH and real-time PCR likely comes from the way the samples were collected. In the FISH method, the samples were immediately fixed, which stops mRNA decay, whereas in the real-time-PCR method, the samples were first centrifuged before cell lysis and RNA extraction, which introduced a delay that was difficult to determine with precision.

MATHEMATICAL MODELING

mRNA intensity profiles obtained for a standard Transcription-Diffusion-Degradation model

We wanted to examine what the spatial profile of mRNA would be if the full-length transcripts were freely diffusible. In the following, we used standard assumptions:

1) Full-length mRNA transcripts diffuse throughout the cell with a diffusion coefficient *D*.

2) The rate of degradation of mRNA is proportional to mRNA concentration, *C,* with rate constant k_{deg} , consistent with the exponential decay of mRNA signal observed in rifampicin-treated cells (Supplementary Fig.2d). We also assume that k_{deg} is spatially uniform in the cytoplasm. Although results presented in this study show patchy RNase E pattern (Fig.6a), those patches are spread around DNA region without particular localization. The mRNA of interest can be degraded at any of these "degradation points". To simplify the model, we substitute actual RNase distribution with the effective uniform one. Using a multi-peak distribution of RNase E does not change significantly mRNA profiles and most importantly, does not change the degree of mRNA localization (data not shown).

3) We assume a simple 1D geometry with reflective boundary conditions at the cell poles located at x=0 and x=3μm and a point source of mRNA at mid cell x_0=1.5μm with constant rate k_{tr}.

Under these conditions, the spatiotemporal dynamic of the mRNA concentration $C(x,t)$ is symmetric around the mid-cell position x_0 and is described by the equation:

$$\partial C(x,t)/\partial t = D\cdot\partial^2 C/\partial x^2 - k_{deg}\cdot C(x,t) \quad [1]$$

with a reflective boundary conditions at $x=l$:

$$\partial C(x=3, t)/\partial x = 0 \quad [2]$$

and a constant influx of transcript at $x=x_0$:

$$-\partial C(x= x_0,t)/\partial x = k_{tr}/(2D) \quad [3]$$

At steady state the solution reads

$$C(x)=k_{tr}\cdot\lambda\cdot [e^{x/\lambda} + e^{-x/\lambda}]/(2\cdot D\cdot\{e^{x0/\lambda} - e^{-x0/\lambda}\}) \quad \text{if } x\leq x_0 \quad [4]$$

$$C(x)=k_{tr}\cdot\lambda\cdot [e^{(l-x)/\lambda} - e^{-(l-x)/\lambda}]/(2\cdot D\cdot\{e^{x0/\lambda} - e^{-x0/\lambda}\}) \quad \text{if } x>x_0$$

where $\lambda=(D/k_{deg})^{1/2}$ characterizes the width of the mRNA spot around the point source. Due to the diffraction limit, the measured signal is a convolution of the mRNA concentration profile from Eq.4 with a point spread function (*PSF*), which we approximate as:

$$PSF(x,s) = I_0\cdot\exp[-(x-s)^2/(2w^2)] \quad [5]$$

where I_0, w, x and s are normalization coefficient, width, coordinate of observation point, and coordinate of point source in image plane, respectively. The w value was obtained by fitting experimentally-determined fluorescence profiles of 175nm-sized red fluorescent beads. The resulting profile is:

$$I(x)=A\cdot\int C(s)\, PSF(x,s)\, ds \quad [6]$$

For the transcription rate, we use k_{tr}=0.06 s^{-1}, which corresponds to approximately 1 transcript per 17 s (this parameter does not influence the spatial distribution of mRNA) and k_{deg}=0.004 s^{-1}, which corresponds to the measured 3.5 min half-time of *groESL-lacO*$_{120}$ mRNA (Supplementary Fig. 2d).

To estimate the diffusion coefficient of mRNA, we consider mRNA as an ideal chain and calculate gyration radius as $R_G=a\cdot(N/6)^{1/2}$ where a is a monomer size and N is a number of monomers[15]. We supposed an "effective monomer size" a=1nm (~ 3 nucleotides), which corresponds to the persistence length of single stranded RNA[16]. Considering chains with N=333 (corresponds to a 1-kb mRNA), 2100 (for the 6.3 kb *groESL-lacO* mRNA) or 6660 (for a 20-kb mRNA), this results in R_G of 8 nm, 19 nm, and 33 nm for free mRNA, respectively. In the case of RNA maximally loaded with

ribosomes, we considered a=20 nm, implying that persistence length is determined by the ribosome to ribosome distance with value obtained from cryo-electron tomograms[17]. This gives: R_G of 34 nm for a 1-kb mRNA, 60 nm for the 6.3-kb *groESL-lacO* mRNA (a=20 nm, N=38 and a=1 nm, N=566 for translated and untranslated portions of the *groESL-lacO* mRNA, respectively), and 150 nm for a 20-kb transcripts.

We used value reported for the diffusion coefficient of GFP molecule within bacterial cell, D_{GFP} =6 $\mu m^2 s^{-1}$ [18], as an estimate a viscosity of the bacterial cytoplasm. Assuming that Stocks radius R_S and R_G of chain are connected as $R_G=(2/5)^{1/2}R_S \approx 0.63 R_S$ (as it would be for solid sphere), and that D equals to $kT/(6\pi\eta R_S)$, we estimated diffusion coefficient as $D=D_{GFP}(0.63R_{GFP}/R_G)$, where R_{GFP}=2.4 nm [19]. This gives estimates D of 1 $\mu m^2 s^{-1}$ for 1-kb free mRNA; 0.5 for 6.3- kb free *groESL-lacO*$_{120}$ mRNA; 0.3 for 20-kb free mRNA; 0.3 for 1-kb mRNA maximally loaded with ribosomes; 0.1 for 6.3- kb *groESL-lacO*$_{120}$ mRNA maximally loaded with ribosomes (in this case, only the 2.3-kb *groESL* portion was considered occupied by ribosomes since the *lacO* array is non-coding); and 0.06 for a long 20-kb mRNA maximally loaded with ribosomes.

Fig. 4a and Supplementary Fig. 6a-b represent expected spatial profiles defined by Eq.6 for these different values of D, assuming a transcription rate of 0.06 s^{-1} and a mRNA degradation rate of 0.004 s^{-1} (corresponding to half-time of 3.5 min). These values resulted in a total of 15 mRNAs per cell. These calculated profiles are essentially uniform throughout the entire cell in sharp contrast with the experimentally observed profiles (Figs. 2a, 2d, 4c and Supplementary Fig 4b, e, h, k). This discrepancy suggests that constraints limit the diffusion of transcripts inside cells.

Experimental determination of the apparent diffusion coefficient (D_a) for *groESL-lacO120* mRNA in heat shocked-treated cells

We determined an apparent diffusion coefficient of mRNA by fitting the Transcription-Diffusion-Degradation model described above to mRNA profiles experimentally obtained in individual cells (see Fig. 4c for examples).

Eq. 6 was fitted to fluorescence mRNA profiles of individual cells using the least square fitting routine *lsqcurvefit* from MATLAB. For each cell, cell length l was determined from corresponding phase image, and A, λ, and x_0 were obtained by fitting.

Since two-peak fluorescence distributions were also observed in experiments (which corresponded to cells with two segregated *groESL-lacO*$_{120}$ gene locus. see Fig. 4c, *left* for example), we also tried to fit each mRNA profile with a model that included two sources of mRNA (each with an independent intensity A and a source location x_0 but with the same λ). To decide whether the one-source or two-source model describes the data best, we assessed the sensitivity of the best fit to the changes in parameters values by calculating the mean relative error $\varepsilon_{av}=(\Sigma(\delta a_i/a_i)^2)/n_p$, where n_p is a number of free parameters in the fitting (n_p=3 and 5 for one-source and two-source models, respectively), δa_i is a confidence interval for the parameter estimate, and a_i is a value of parameter with summation over all parameters. The model with the highest sensitivity to changes in the parameters was chosen (fluorescence profiles that gave ε_{av}>0.5 for both one-source and two-source models were excluded from the analysis).

This procedure was applied to each fluorescence profiles resulting in λ=0.37±0.1 μm averaged from two independent experiments (n= 1,717 and 974 individual cells). The relative accuracy of individual λ estimates ($\delta\lambda/\lambda$) ranged from 0.14 to 0.8 for more than 80% of analyzed cells. Taking into account the measured degradation rate k_{deg}=0.004 s^{-1} (from Supplementary Fig. 2d), λ=0.37 μm gives an estimate for D_a of 0.0005±0.0003 μm^{2}s^{-1}.

SUPPLEMENTARY TABLES

Table S1. Strain and plasmid table

Strain	Relevant Genotype or Description	Reference or Source
***C. crescentus* strains**		
CB15N	Synchronizable variant of CB15 (also NA1000)	[20]
CJW2555	CB15N *vanA*::pHL23Pvan-mcherrybs48tm *xylX*::pBGentPxylMS2dmGFP	This study
CJW2556	CB15N *xylX*::pBGentPxylMS2(dlFG)mGFP	This study
CJW2560	CB15N *vanA*::pHL23Pvan-mcherrybs48tm *xylX*::pBGentPxylMS2(dlFG)mGFP	This study
CJW2780	CB15N *xylX*::pBGentPxylMS2dmGFP	This study
CJW2781	CB15N *xylX*::pHPV543::pBGentPxylMS2(dlFG)-mcherry	This study

CJW2783	CB15N *divJ*::pHL23divJc-bs48-3'UTR::pBAp-LacO *xylX*::pHPV543::pBGentPxylMS2(dlFG)mcherry	This study
CJW2966	CB15N *groESL*::pHL23groESL-lacO$_{120}$tm	This study
CJW2967	CB15N *creS*::pHL23creS-lacO$_{120}$tm	This study
CJW2968	CB15N *divJ*::pHL23divJ-lacO$_{120}$tm	This study
CJW2969	CB15N *groESL*::pHL23groESL-lacO$_{120}$tm *xylX*::pHPV543 (*Pxyl lacI-cfp*)	This study
CJW3093	CB15N *ompA*::pHL23ompA-lacO$_{120}$tm	This study
CJW3097	CB15N *vanA*::pHL23-Pvan-mcherry-lacO$_{120}$tm	This study
CJW3099	CB15 divD308(Ts)::pDW110 divE309(Ts)	This study
CJW3100	CB15N *rne*::pHL23rne-mgfp	This study
CJW3102	CB15N *Cori*::Cori(tetO)pGENT *xylX*::pHPV472 *creS*::pHL23creS-lacO$_{120}$tm	This study
CJW3364	CB15N *fljK*::pHL23fljK-lacO$_{120}$tm	This study
CJW3365	CB15N *rplA*::pL1-GFPC-1	This study
LS3812	CB15N Δ*creS*	[21]
MT16	CB15N *Cori*::Cori(tetO)pGENT *xylX*::pHPV472 carrying a translational fusion of *lacI-cfp* and *tetR-yfp* under the control of *Pxyl*	[22]
PC6340	CB15 divD308(Ts)::pDW110 divE309(Ts) carrying ts mutation in *ftsA* and *parE*	[23]
PV3153	CB15N *xylX*::pHPV543 carrying *lacI-cfp* under the control of P*xyl*	P. Viollier
***E. coli* strains**		
DH5α	Cloning strain	Invitrogen
DL2875	MG1655 *lacIq lacZ*χ$^-$ cynX::(tetO)250 (Gent^R)	[24]
MG1655	F$^-$ λ$^-$ *ilvG- rfb-50 rph*-1	K. Gerdes
SM10	M294::RP4-2 (Tc::Mu); for plasmid mobilization	[25]
S17-1	M294::RP4-2 (Tc::Mu)(Km::Tn*7*); for plasmid mobilization	[25]
Plasmids		
pBAp	Integration plasmid (Apramycin^R)	This study
pBAp-LacO	pBAp carrying an array of 240 *lacO* sites	This study
pBGent	Integration plasmid (Gent^R)	[26]
pBGent-LacO$_{240}$	pBGent carrying the *lacO$_{240}$* array	This study
pBGentPxylMS2dmGFP	pBGent carrying *ms2d-mgfp* under control of *Pxyl*	This study
pBGentPxylMS2(dlFG)mGFP	pBGent integration vector carrying *ms2-mgfp* under control of *Pxyl*	This study
pBGentPxylMS2(dlFG)mCherry	pBGent carrying *ms2-mCherry* under control of *Pxyl*	This study
pBGS18	Integrating plasmid (Kan^R)	D. Alley
pCR2.1-TOPO	Amp^R Kan^R PCR cloning vector	Invitrogen

pCT119 dlFG	Amp^R plasmid producing MS2 with deletion of the FG loop, rendering it assembly-defective	[27]
pGFPC-1	Integration plasmid (Spec/StrepR) to create GFP C-terminal fusions, integrated at the site of interest	[12]
pHL23	Integration plasmid (Kan^R)	[28]
pHL23creS-lacO120tm	pHL23 carrying the 3'-end of *creS* transcriptionally fused to $lacO_{120}$, with an additional *E. coli trpA* terminator	This study
pHL23divJc-bs48-3'UTR	pHL23 carrying 3'end of *divJ* transcriptionally fused to *bs48* and *divJ* 3'UTR to create *divJ-bs48-3'UTR* under native promoter	This study
pHL23divJ-$lacO_{120}$tm	pHL23 carrying the 3'-end of *divJ* transcriptionally fused to $lacO_{120}$, with an additional *E. coli trpA* terminator	This study
pHL23fljK-$lacO_{120}$tm	pHL23 carrying the 3'end of *fljK* transcriptionally fused to $lacO_{120}$ with an additional transcriptional *E. coli trpA* terminator	This study
pHL23groESL-$lacO_{120}$tm	pHL23 carrying the 3'-end of *groESL* transcritionally fused to $lacO_{120}$, with an additional *E. coli trpA* terminator	This study
pHL23ompA-$lacO_{120}$tm	pHL23 carrying the 3'-end of *ompA* transcriptionally fused to $lacO_{120}$ and *E. coli trpA* terminator	This study
pHL23Pvan-mcherrybs48tm	pHL23 carrying *mcherry-bs48* under control of *Pvan*	This study
pHL23Pvan-mcherry-$lacO_{120}$tm	pHL23 carrying *mcherry* under the control of *Pvan* and transcriptionally fused to $lacO_{120}$ and *E. coli trpA* terminator	This study
pHL23rne-mgfp	pHL23 carrying the 3'-end of *rne* translationally fused to *mgfp*	This study
pHL32	Integration plasmid (Kan^R)	[28]
pHL32Pvan-mcherry	pHL32 carrying *mcherry* under the control of *Pvan*	This study
pHP45Ω aaC4	Amp^R $Apramycin^R$ cloning vector	[29]
pIG-BS48-I	pKS vector with an array of 48 MS2 binding sites	[3]
pIG-E133-2cTG	ColE1-based expression vector (Kan^R) carrying *ms2d-gfp*	[2]
pKS	Amp^R cloning vector	Stratagene
pKScreS-R	Coding sequence, 5'UTR and 3'UTR of *creS* cloned from the *C. crescentus* genome	N. Ausmees
pKSdivJ	Coding sequence and 5'UTR of *divJ* cloned from the *C. crescentus* genome	H. Lam

pKSgroEL480	pKS carrying a 3'-end fragment of *groEL* cloned from the *C. crescentus* genome.	This study
pKS(pleD3'UTR)tm	pKS carrying the 3'UTR of *pleD* fused to *E. coli trpA* terminator	This study
pKS(lacO)120tm	pKS carrying $lacO_{120}$ fused to *E. coli trpA* terminator	This study
pKSmCherry-N2	pKS carrying *mcherry* in the N-2 frame	P. Angelastro
pKSmgfp-N1	pKS carrying *mgfp* in the N-1 frame	P. Angelastro
pLAU38	Amp^R Kan^R pUC18 derivative plasmid with an array of 120 lacO sequences	[30]
pLAU43	Amp^R Kan^R pUC18 derivative plasmid with an array of 240 *lacO* sequences	[30]
pL1-GFPC-1	PGFPC-1 carrying a 3'-end fragment of *rplA* cloned from the *C.crescentus* CB15N genome	This study
pNJH17	Integrating vector (Kan^R) carrying *ftsZ-mcherry* under the control of *Pvan*	N. Hillson
pRW431	Amp^R and Kan^R cloning vector carrying 500bp region that includes *Pxyl*	R. Wright

Table S2. Percentage of cells with fluorescent spots after RNA FISH

mRNA	Number of cells	Cells with spots (%)	Cells without spots (%)	Cells with 1 spot (%)	Cells with 2 spots (%)	Cells with > 2 spots (%)
groESL-$lacO_{120}$ (normal growth)	1508	79.3±1.3	20.7±1.3	56.6±0.8	23.9±0.07	0.9±0.3
groESL-$lacO_{120}$ (heat shock)	2364	95.3±2.2	4.7±2.2	41.3±3.7	37.4±1.9	16.5±0.5
lacZ	995	93.3±3	6.75±3	30.8±7.4	51.9±5.7	10.6±4.7

The foci were identified using SpotFinder (described above). The errors correspond to the standard deviation for at least 2 experiments. The *groESL-*$lacO_{120}$ mRNA signal was visualized in *C. crescentus* CJW2966 strain after growth at 30˚C (normal growth) and after heat shock at 42˚C for 15 min using the lacO probe, whereas the native *lacZ* mRNA signal was visualized in *E. coli* MG1655 after IPTG induction for 20 min using 48 probes complementary to the *lacZ* coding sequence.

CONSTRUCTION OF PLASMIDS

pBAp: Plasmid pBGST18 was digested with MluI to remove the kanamycin resistance-encoding cassette. The apramycin resistance-encoding cassette was removed from pHP45ΩaacC4 with BamHI (blunted) and cloned into the prepared pBGST18 vector to create pBAp.

pBAp-LacO: An XbaI/NheI fragment containing the *lacO*$_{240}$ array was cut out of plasmid pLAU43 and cloned into pBAp digested with XbaI. The kanamycin resistance cassette was removed from the resulting plasmid with an NsiI digest and re-ligated to create pBAp-LacO.

pBGentPxylMS2dmGFP: MS2d was cut out of plasmid pIG-E133-2cTG using enzyme BamHI and subcloned into pKS, digested with the same enzyme. MS2d was then PCR amplified with forward primer 5'TAGACTAGTGGATCCCATATGGCTTCT3', and reverse primer 5'ACTGCAGAAGGGGGATCCGTAGAT3', adding an NdeI site at the 5' end and a PstI site at the 3' end, and sequence verified. An EcoRV/NdeI Pxyl fragment from pRW431, an NdeI/PstI MS2d fragment, and a PstI/XbaI mGFP fragment were cloned into pBGent digested with PstI (blunted) and XbaI.

pBGentPxylMS2mcherry: The 0.8kb HindIII/BamHI PxylMS2 fragment from pBGentPxylMS2mGFP, and the 0.8kb BamHI/XbaI mCherry fragment from pKSmCherry-N2 were cloned into pBGent vector digested with HindIII/XbaI.

pBGentPxylMS2mGFP: A 0.4kb MS2 fragment was PCR amplified from pCT119 with forward primer 5'TAGACTAGTGGATCCCATATGGCTTCT3', and reverse primer 5'ACTGCAGAAGGGGGATCCGTAGAT3', adding an NdeI site at the 5' end and a PstI site at the 3' end, and sequence verified. An EcoRV/NdeI Pxyl fragment from pRW431, an NdeI/PstI MS2 fragment, and a PstI/XbaI mGFP fragment were cloned into pBGent restricted with PstI (blunted) and XbaI.

pHL23creS-lacO$_{120}$tm: plasmid pHL32creS was digested with StuI and XbaI and the 800 bp fragment containing the 3'-end of *creS* was gel purified. Plasmid pKSlacO$_{120}$tm

was digested with NheI and HindIII and the 4.5 Kb *lacO*$_{120}$tm fragment was gel purified. A triple digestion was set between pHL23 digested with EcoRV and HindIII, *creS* 3'end digested with StuI and XbaI, and *lacO*$_{120}$tm digested with NheI and HindIII. The correct construct was verified by restriction analysis and sequencing.

pHL23divJ-lacO$_{120}$tm: plasmid pKSdivJ was digested with NotI and SmaI, and the 2 Kb fragment was gel purified (*divJ* 3'end). In parallel, the pKSlacO$_{120}$tm was digested with NheI, blunted with Klenow and digested with HindIII. The 4.5 Kb *lacO*$_{120}$tm fragment was gel purified. A triple ligation was set between pHL23 digested with NotI and HindIII, the *divJ* fragment (NotI and SmaI ends), and the *lacO*$_{120}$tm array (Blunt and HindIII). The correct construct was verified through restriction analysis and sequencing.

pHL23divJc-bs48-3'UTR: 300bp of the *divJ* 3' UTR was cloned out of the genome with forward primer 5'TTTAAGCTTACGCCCGACCGGCGGCGAAGTCTC3' and reverse primer 5'TTTGTCGACATTCTGCGCGACACCAAG3', adding a HindIII and SalI site, respectively, and sequence verified. A 1.4kb 3' *divJ* fragment was cut out of pKSdivJ with NotI/BamHI(blunted) and ligated to an XbaI(blunted)/HindIII *bs48* fragment from pIG-BS48-I, and the HindIII/SalI *divJ* 3'UTR fragment, in the vector backbone pHL23 restricted with NotI and SalI.

pHL23fljK-lacO120tm: A 600 bp containing the 3'-end of *fljK* was PCR amplified from *C.crescentus* genomic DNA using primers fljK-SacI For (5' ATATGAGCTCTGAAGGACTCGCTGCAA3') and fljK-NheI Rev (5' CGCGGCTAGCTTAACGGAACAGGCTCA). The PCR product was digested using enzymes SacI and NheI. The 4.5kb *lacO*$_{120}$*tm* fragment was cut out from plasmid pKSlacO$_{120}$tm using enzymes NheI and HindIII. The two fragments were inserted into plasmid pHL23 cut with SacI and HindIII. The correct construct was verified by restriction analysis and sequencing.

pHL23groEL-lacO$_{120}$tm: The 1.2Kb 3'-end *groEL* fragment was cut out of plasmid pKSgroEL480 using enzymes SacI and XbaI. The 4.5Kb *lacO*$_{120}$tm fragment was cut out

of plasmid pKSlacO_{120}tm using enzymes NheI and HindIII. The two fragments were gel purified and inserted into plasmid pHL23 digested with enzymes SacI and HindIII. The correct construct was verified through restriction analysis and sequencing.

pHL23ompAlacO_{120}tm: A 800 bp fragment containing the 3'-end of *ompA* was PCR amplified using *C. crescentus* genome DNA as template and primers ompA-SacI-up (5' GCGCGAGCTCCAACCTCATCTTCGACAT3') and ompA-NheI-down (5' GCGCGCTAGCTTATTGGAAGTTGATCGAG). The PCR product was gel purified and was digested using enzymes SacI and NheI. The 4.5kb *lacO_{120}tm* fragment was cut out from plasmid pKSlacO_{120}tm using enzymes NheI and HindIII. The two fragments were inserted into plasmid pHL23 cut with SacI and HindIII. The correct construct was verified by restriction analysis and sequencing.

pHL23PvanCHY lacO_{120}tm: The 1.8 kb fragment containing the inducible promoter *Pvan* fused to *mcherry* was cut out of plasmid pHL32Pvan-mcherry using enzymes XbaI and EcoRV and was gel purified. Plasmid pKSlacO_{120}tm was cut using enzyme NheI and the cohesive ends were blunted using Klenow. This plasmid was then digested with HindIII, and the 4.5 kb *lacO_{120}*tm fragment was gel purified. A triple ligation was set between fragments Pvan-mcherry and *lacO_{120}*tm to insert into plasmid pHL23 digested with enzymes XbaI and HindIII. The correct plasmid was verified by restriction analysis and sequencing.

pHL23PvanmCherrybs48tm: pKSdivJ3'UTRtm was digested with HindIII and SalI to remove the *divJ* 3'UTR fragment, both ends blunted and re-ligated to create pKStm. pHL23bs48tm was created by cutting out the terminator from pKStm with SmaI/KpnI, cutting out a bs48 fragment with BamHI/HindIII (blunted), and cloning into pHL23 restricted with BamHI / KpnI. A *mcherry* fragment was cloned by PCR from pNJH17 with NdeI/EcoRV at the ends, and cloned to *Pvan* fragment cut out of pNJH17 with XbaI/NdeI into a pHL32 vector restricted with XbaI/EcoRV. Then the *Pvan-mcherry* fragment was cut out with XbaI/EcoRV and cloned to bs48tm cut with XbaI(blunted)/KpnI into pHL32 restricted with XbaI/KpnI.

pHL23rne-mgfp: The 3'end of *rne* was PCR amplified from *C. crescentus* genomic DNA using primers rne(800)-SacI (5'GCGCGAGCTCTACGACAAGGACCTGGAC) and rne(stop)-KpnI (5'ATATGGTACCCCGGCGCCACCA). The 800bp amplicon was then digested with enzymes SacI and KpnI. Fragment *mgfp* was cut out from plasmid pKS-mgfp N1 using enzymes KpnI and XbaI. The 900 bp *mgfp* fragment was gel purified. Both fragments were inserted into plasmid pHL23 digested with enzymes SacI and XbaI.

pHL32Pvan-mcherry: A DNA fragment of the *mcherry* coding sequence was amplified by PCR using pNJH17 as a template and primers mCherrybs48FOR (5'AAACATATGGTGAGCAAGGGCGAGGAGGAT) and Cherrybs48REV (5'AAAGATATCTTACTTGTACAGCTCGTCCAT), which add NdeI and EcoRV sites at the ends. This PCR product and a XbaI/NdeI DNA fragment of pNJH17 containing *Pvan* were triple ligated into a pHL32 vector cut with XbaI/EcoRV.

pKS$lacO_{120}$tm: The 4.5 kb $lacO_{120}$ fragment was cut out of plasmid pLAU38 using enzymes BamHI and SalI. The 4.5 Kb fragment $lacO_{120}$ array was gel purified. To add the *trpA* additional terminator, the plasmid pKS(pleD3'UTR)tm was digested with enzymes Sal I and KpnI. The enzymes were heat inactivated and a triple ligation was set between pKS (digested with BamHI and KpnI), the $lacO_{120}$ fragment (digested with BamHI and SalI) and the digestion mixture of pKS(pleD3'UTR)tm (the *trpA* terminator is too small to gel purify it). The correct constructs were verified by restriction analysis and sequencing.

pKS(pleD3'UTR)tm: The 3'UTR region of *pleD* was PCR amplified from *C. crescentus* genomic DNA using primers DivK3UTR FOR (5'CCGAAGCTTGAGCGGGCGCCCAG) and DivK 3UTR REV (5'ACGCGTCGACGACTGATAGCCGTTCGGATA). The 350

bp fragment was inserted into plasmid pKS digested with EcoRV and treated with antarctic phosphatase. The *trpA* transcriptional terminator was added by PCR amplification using the primers DivK 3UTR FOR and DivK 3'UTR ttm (5'CGGGGTACCAAGAAAAAAAAGCCCGCTCATTAGGCGGGCACGCGTCGACG ACT). The 400 bp fragment was inserted into plasmid pKS digested with EcoRV and treated with phosphatase. The correct clone was verified by sequencing.

pKSgroEL480: The 3'end of *groEL* was PCR amplified from *C. crescentus* genomic DNA using primers groEL480-For-SacI (GCGCGAGCTCATGATCGCCAAGGCCAT) and groEL1644Rev-XbaI (GCGCTCTAGACCTTAGAAGTCCATGT). The 1.2kb amplicon was inserted into cloning plasmid pKS digested with EcoRV. The correct construct was verified by restriction analysis and sequencing.

pL1-GFPC-1: The 3'end of *rplA* was PCR amplified from CB15N genomic DNA using primers L1-Forward (ATATAAGCTTGAGATCTCGGTCAACCT) and L1 (no stop)-Rev (ATATGGTACCGGCGCCGATCGAGCTGATGT). The 700 bp fragment was cut with enzymes HindIII and KpnI and inserted into pGFPC-1 digested with the same enzymes. The correct construct was verified by restriction analysis and sequencing.

CONSTRUCTION OF STRAINS

CJW2555: pHL23PvanmCherrybs48tm was integrated into the *vanA* locus of CB15N by transformation and the *vanA*::pHL23PvanmCherrybs48tm locus was moved by ΦCR30 phage transduction into CJW2780.

CJW2556: pBGentPxylMS2mGFP was integrated into the *xylX* locus of CB15N by transformation.

CJW2560: pHL23PvanmCherrybs48tm was integrated into the *vanA* locus of CB15N by transformation and the *vanA*::pHL23PvanmCherrybs48tm locus was moved by ΦCR30 phage transduction into CJW2556.

CJW2780: pBGentPxylMS2dmGFP was integrated into the *xylX* locus of CB15N by transformation.

CJW2781: S17-1 cells carrying pBGentPxylMS2mCherry were mated to CJW1215.

CJW2783: pHL23divJc-bs48-3'UTR was integrated into the *divJ* locus of CB15N as the only copy of *divJ* in the genome and ΦCR30 phage lysate of CJW2781 was transduced into the resulting strain to make CJW2783.

CJW2966: Plasmid pHL23groELlacO$_{120}$tm was introduced into wild-type CB15N cells by conjugation with S17-1 *E. coli* strain. Integration occurred at the *groESL* gene locus.

CJW2967: Plasmid pHL23creSlacO$_{120}$tm was introduced into wild-type CB15N cells by conjugation with S17-1 *E. coli* strain. Integration occurred at the *creS* gene locus.

CJW2968: Plasmid pHL23divJlacO$_{120}$tm was introduced into wild-type CB15N cells by conjugation with S17-1 *E. coli* strain. Integration occurred at the *divJ* gene locus.

CJW2969: A ΦCR30 transducing phage lysate carrying *xylX*::pHPV543 (Kan^R) was obtained from strain CJW1215. *xylX*::pHPV543 was transduced into strain CJW2966. The synthesis of LacI-CFP was verified by microscopy after induction with 0.3% xylose.

CJW3093: Plasmid pHL23ompAlacO$_{120}$tm was introduced into CB15N cells by conjugation with S17-1 *E. coli* strain. Integration occurred at the *ompA* gene locus.

CJW3096: A ΦCR30 phage lysate carrying *groESL*::pHL23groESLlacO$_{120}$tm was obtained from strain CJW2966. *groESL*::pHL23groESLlacO$_{120}$tm was transduced into strain CJW3101. The resulting strain requires xylose for growth.

CJW3097: Plasmid pHL23Pvan-mcherrylacO$_{120}$tm was introduced into CB15N cells by conjugation with S17-1 *E. coli* strain. Integration occurred at the *vanA* gene locus.

CJW3099: A ΦCR30 phage lysate carrying *rne*::pHL23rne-mgfp was obtained from strain CJW3100. *rne*::pHL23rne-mgfp was transduced into strain CJW2673.

CJW3100: Plasmid pHL23rne-mgfp was introduced into CB15N cells by conjugation with S17-1 *E. coli* strain. Integration occurred at the *rne* gene locus.

CJW3102: A ΦCR30 phage lysate carrying *creS*::pHL23creSlacO_{120}tm was obtained from strain CJW2967. *creS*::pHL23creSlacO_{120}tm was transduced into strain CJW1059.

CJW3364: Plasmid pHL23fljK-lacO_{120}tm was introduced into CB15N cells by electroporation. Integration occurred at the *fljK* gene locus.

CJW3365: Plasmid pL1-GFPC-1 was introduced into CB15B cells by conjugation with SM10 *E. coli* strain. Integration occurred at the *rplA* gene locus.

List of DNA probes used for RNA FISH of endogenous mRNAs

For *creS* mRNA

5’ [Cy3]ATCAAGGCGATCTGGCGCTGGGCCTG

5’ [Cy3]GCGAGGCGGGCGGAAACCTCGCGTTCCT

5’ [Cy3]GCGTCGGATTCGCCGAGCGCCGTTTC

5’ [Cy3]CGTTGTCTTCCAGCGCCGCGTCCTGGGTCTG

5’ [Cy3]CAGCAGGGCGTTGCGCAGGCGGTCGATCT

5’ [Cy3]AGGCGTCGAGGCTGGAGACCTTCAGGT

5’ [Cy3]AGGTGCTCGATGCGGGCGGTGGCGTCG

5’ [Cy3]CTGGGCCTGGACGCGCAGGCCTTCGACGT

5’ [Cy3]GCCTCGGCGTCGCCACGGCGAGCGT

5’ [Cy3]AGGGCGTTGTCCTGGTTGGCGCGAG

5’ [Cy3]ACGCGCTTCTTCAGCGTCGCGGCTTCCTC

5’ [Cy3]ATAGGCGGGCCAGGTCCAGCCCGGCCT

5’ [Cy3]CAGCTGGGCTTCAAGATCGGTTTCGAT

5’ [Cy3]CGTTTTCGACGGCCTGAACGCGGGCGCGCT

5’ [Cy3]CGGATCGTGCGACCGCTGTCGGCCTGATGC

5’ [Cy3]GCGGTTGGCCTCGACCTGGCTTTCCA

5’ [Cy3]TCTCCAGGCGCGTCTGCAGAGCGGAGAT

5’ [Cy3]CATCTCTTCCAGCTTGTCGGCGCGACCCGT

5’ [Cy3]CTGGAGTCGGCGAGACGGGCCGAGATCT

5’ [Cy3]GCGCGGCGTTCCACCGCCTTCTGCT

5’ [Cy3]AGGGCGCGCTCCAGGGCGACATTGAGAT

5’ [Cy3]TCAGCCTCTTCCTCCAGGGCCCGGAT

5’ [Cy3]CGGTGTCGACGCCGGCGTGACGCTGGC

5’ [Cy3]CAGCTGGTCGGCGCGTTCGATGGCCGT

5’ [Cy3]TTGAGGGCCTTTTCTTGCGCCACAGCGCT

5’ [Cy3]CGATCTTCGCCTCGTGATCGCGGCGAA

5’ [Cy3]CTTCCGAGGTCAGGCGCTCGATGGTCGCCT

5’ [Cy3]GGCGGCTTCCAGGGCCCCTTCGGCCA

5’ [Cy3]AGCAGGGCCATCTGCAGGCGTGAGCGGT

5’ [Cy3]TTAGGCGCTCGCGGCCACGTCGCCGTCGCT

For *lacZ* mRNA

5’ [Cy3]GCCAGTGAATCCGTAATCATGGTCA

5’ [Cy3]GGTTTTCCCAGTCACGACGTTGTAA

5’ [Cy3]CTGCAAGGCGATTAAGTTGGGTAAC

5’ [Cy3]TTCGCTATTACGCCAGCTGGCGAAA

5’ [Cy3]ATTCAGGCTGCGCAACTGTTGGGAA

5’ [Cy3]TTCTGGTGCCGGAAACCAGGCAAAG

5’ [Cy3]AAGATCGCACTCCAGCCAGCTTTCC

5’ [Cy3]AGTTTGAGGGGACGACGACAGTATC

5’ [Cy3]TTGGTGTAGATGGGCGCATCGTAAC

5’ [Cy3]ACGGCGGATTGACCGTAATGGGATA

5’ [Cy3]AGTAACAACCCGTCGGATTCTCCGT

5’ [Cy3]CCTGTAGCCAGCTTTCATCAACATT

5’ [Cy3]CGCCATCAAAAATAATTCGCGTCTG

5’ [Cy3]CGTTGCACCACAGATGAAACGCCGA

5’ [Cy3]AAACGACTGTCCTGGCCGTAACCGA

5’ [Cy3]CGCGTAAAAATGCGCTCAGGTCAAA

5’ [Cy3]AGCACCATCACCGCGAGGCGGTTTT

5’ [Cy3]TCTTCCAGATAACTGCCGTCACTCC

5’ [Cy3]AAAATGCCGCTCATCCGCCACATAT

5’ [Cy3]GTCGGTTTATGCAGCAACGAGACGT

5’ [Cy3]GAGTGGCAACATGGAAATCGCTGAT

5’ [Cy3]GTACAGCGCGGCTGAAATCATCATT

5’ [Cy3]AACTCGCCGCACATCTGAACTTCAG

5’ [Cy3]CCTGCCATAAAGAAACTGTTACCCG

5’ [Cy3]TCGATAATTTCACCGCCGAAAGGCG

5’ [Cy3]TAGTGTGACGCGATCGGCATAACCA

5’ [Cy3]CCACAGTTTCGGGTTTTCGACGTTC

5’ [Cy3]CGCACGATAGAGATTCGGGATTTCG

5’ [Cy3]ATCGCAGGCTTCTGCTTCAATCAGC

5’ [Cy3]ATTTTCAATCCGCACCTCGCGGAAA

5’ [Cy3]ATCAGCAACGGCTTGCCGTTCAGCA

5’ [Cy3]GGATGATGCTCGTGACGGTTAACGC

5’ [Cy3]GTCTGCTCATCCATGACCTGACCAT

5’ [Cy3]TGCTTCATCAGCAGGATATCCTGCA

5’ [Cy3]AATGCGAACAGCGCACGGCGTTAAA

5’ [Cy3]ACAGCGTGTACCACAGCGGATGGTT

5’ [Cy3]TTCATCCACCACATACAGGCCGTAG

5’ [Cy3]TGGCACCATGCCGTGGGTTTCAATA

5’ [Cy3]TAGCCAGCGCGGATCATCGGTCAGA

5’ [Cy3]CATTCGCGTTACGCGTTCGCTCATC

5’ [Cy3]ATCACACTCGGGTGATTACGATCGC

5’ [Cy3]ATTAGCGCCGTGGCCTGATTCATTC

5’ [Cy3]AGATTTGATCCAGCGATACAGCGCG

5’ [Cy3]TTCATACTGCACCGGGCGGGAAGGA

5’ [Cy3]AATAATATCGGTGGCCGTGGTGTCG

5’ [Cy3]GTCTTCATCCACGCGCGCGTACATC

5’ [Cy3]TGGACCATTTCGGCACAGCCGGGAA

5’ [Cy3]TCTCTCCAGGTAGCGAAAGCCATTT

List of LNA probes used for FISH

lacO: 5’ [Cy3] or [FITC]AATTGTTATCCGCTCAC

lacO Reverse: 5' [FITC]GTGAGCGGATAACAATT

tetO: 5' [Alexa488]CTCTATCACTGATAGGGA

groESL: 5'[Cy3]GTCGGAGGAGAAATAGACGTCTTTA

REFERENCES

1. Bertrand, E. et al. Localization of ASH1 mRNA particles in living yeast. *Mol Cell* 2, 437-45 (1998).
2. Golding, I. & Cox, E. C. RNA dynamics in live Escherichia coli cells. *Proc Natl Acad Sci U S A* 101, 11310-5 (2004).
3. Golding, I., Paulsson, J., Zawilski, S. M. & Cox, E. C. Real-time kinetics of gene activity in individual bacteria. *Cell* 123, 1025-36 (2005).
4. Bernstein, J. A., Khodursky, A. B., Lin, P. H., Lin-Chao, S. & Cohen, S. N. Global analysis of mRNA decay and abundance in Escherichia coli at single-gene resolution using two-color fluorescent DNA microarrays. *Proc Natl Acad Sci U S A* 99, 9697-702 (2002).
5. Lim, F. & Peabody, D. S. Mutations that increase the affinity of a translational repressor for RNA. *Nucleic Acids Res* 22, 3748-52 (1994).
6. Ebersbach, G., Briegel, A., Jensen, G. J. & Jacobs-Wagner, C. A self-associating protein critical for chromosome attachment, division, and polar organization in caulobacter. *Cell* 134, 956-68 (2008).
7. Kirstein, J., Strahl, H., Moliere, N., Hamoen, L. W. & Turgay, K. Localization of general and regulatory proteolysis in Bacillus subtilis cells. *Mol Microbiol* 70, 682-94 (2008).
8. Peabody, D. S. Translational repression by bacteriophage MS2 coat protein expressed from a plasmid. A system for genetic analysis of a protein-RNA interaction. *J Biol Chem* 265, 5684-9 (1990).
9. Femino, A. M., Fay, F. S., Fogarty, K. & Singer, R. H. Visualization of single RNA transcripts in situ. *Science* 280, 585-90 (1998).
10. Maamar, H., Raj, A. & Dubnau, D. Noise in gene expression determines cell fate in Bacillus subtilis. *Science* 317, 526-9 (2007).
11. Raj, A., van den Bogaard, P., Rifkin, S. A., van Oudenaarden, A. & Tyagi, S. Imaging individual mRNA molecules using multiple singly labeled probes. *Nat Methods* 5, 877-9 (2008).
12. Thanbichler, M., Iniesta, A. A. & Shapiro, L. A comprehensive set of plasmids for vanillate- and xylose-inducible gene expression in Caulobacter crescentus. *Nucleic Acids Res* 35, e137 (2007).
13. Cootes, T. F., Taylor, C. J., Cooper, D. H. & Graham, J. Active Shape Models - Their Training and Application. *Computer Vision and Image Understanding* 61, 38-59 (1995).
14. Pfaffl, M. W. A new mathematical model for relative quantification in real-time RT-PCR. *Nucleic Acids Res* 29, e45 (2001).
15. Yamakawa, H. Modern Theory of Polymer Solutions. *Harper & Row* New York (1971).

16. Seol, Y., Skinner, G. M. & Visscher, K. Elastic properties of a single-stranded charged homopolymeric ribonucleotide. *Phys Rev Lett* 93, 118102 (2004).
17. Brandt, F. et al. The native 3D organization of bacterial polysomes. *Cell* 136, 261-71 (2009).
18. Slade, K. M., Baker, R., Chua, M., Thompson, N. L. & Pielak, G. J. Effects of recombinant protein expression on green fluorescent protein diffusion in Escherichia coli. *Biochemistry* 48, 5083-9 (2009).
19. Uskova, M. A. et al. Fluorescence dynamics of green fluorescent protein in AOT reversed micelles. *Biophys Chem* 87, 73-84 (2000).
20. Evinger, M. & Agabian, N. Envelope-associated nucleoid from Caulobacter crescentus stalked and swarmer cells. *J Bacteriol* 132, 294-301 (1977).
21. Gitai, Z., Dye, N. & Shapiro, L. An actin-like gene can determine cell polarity in bacteria. *Proc Natl Acad Sci U S A* 101, 8643-8 (2004).
22. Viollier, P. H. et al. Rapid and sequential movement of individual chromosomal loci to specific subcellular locations during bacterial DNA replication. *Proc Natl Acad Sci U S A* 101, 9257-62 (2004).
23. Ward, D. & Newton, A. Requirement of topoisomerase IV parC and parE genes for cell cycle progression and developmental regulation in Caulobacter crescentus. *Mol Microbiol* 26, 897-910 (1997).
24. White, M. A., Eykelenboom, J. K., Lopez-Vernaza, M. A., Wilson, E. & Leach, D. R. Non-random segregation of sister chromosomes in Escherichia coli. *Nature* 455, 1248-50 (2008).
25. Simon, R., Prieffer, U. & Puhler, A. A broad host range mobilization system for *in vivo* genetic engineering: Transposon mutagenesis in gram negative bacteria. *Biotechnology* 1, 784-790 (1983).
26. Matroule, J. Y., Lam, H., Burnette, D. T. & Jacobs-Wagner, C. Cytokinesis monitoring during development; rapid pole-to-pole shuttling of a signaling protein by localized kinase and phosphatase in Caulobacter. *Cell* 118, 579-90 (2004).
27. Peabody, D. S. & Ely, K. R. Control of translational repression by protein-protein interactions. *Nucleic Acids Res* 20, 1649-55 (1992).
28. Lam, H., Schofield, W. B. & Jacobs-Wagner, C. A landmark protein essential for establishing and perpetuating the polarity of a bacterial cell. *Cell* 124, 1011-23 (2006).
29. Blondelet-Rouault, M. H., Weiser, J., Lebrihi, A., Branny, P. & Pernodet, J. L. Antibiotic resistance gene cassettes derived from the omega interposon for use in E. coli and Streptomyces. *Gene* 190, 315-7 (1997).
30. Lau, I. F. et al. Spatial and temporal organization of replicating Escherichia coli chromosomes. *Mol Microbiol* 49, 731-43 (2003).